Supporting Information

Cobalt-substituted $SrTi_{0.3}Fe_{0.7}O_{3-\delta}$: a stable high-performance oxygen electrode material for intermediate-temperature solid oxide electrochemical cells

Shan-Lin Zhang,[ab], Hongqian Wang,[a] Matthew Y. Lu,[a] Ai-Ping Zhang,[b] Liliana V. Mogni,[c] Qinyuan Liu,[a] Cheng-Xin Li,[b] Chang-Jiu Li,[b]* and Scott A. Barnett [a]*

[a] Department of Materials Science and Engineering, Northwestern University, Evanston, Illinois 60208, USA

[b] State Key laboratory for Mechanical Behavior of Materials, School of Materials Science and Engineering, Xi'an Jiaotong University, Xi'an, Shaanxi, 710049, People's Republic of China

[c] CONICET-CNEA, Centro Atomico Bariloche, Av. Bustillo 9500, CP 8400, S.C. Bariloche, Argentina

*Corresponding author. licj@xjtu.edu.cn, s-barnett@northwestern.edu

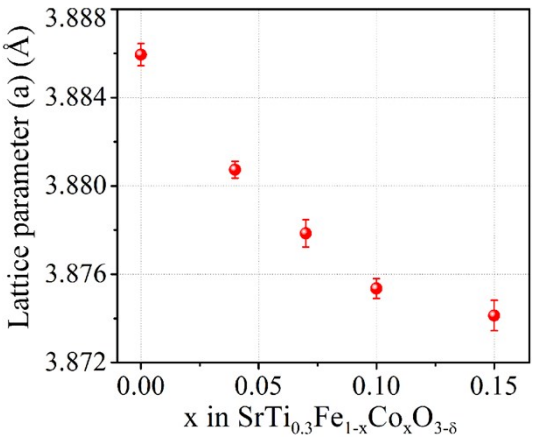

Fig. S1 Variation in lattice parameter with cobalt substitution.

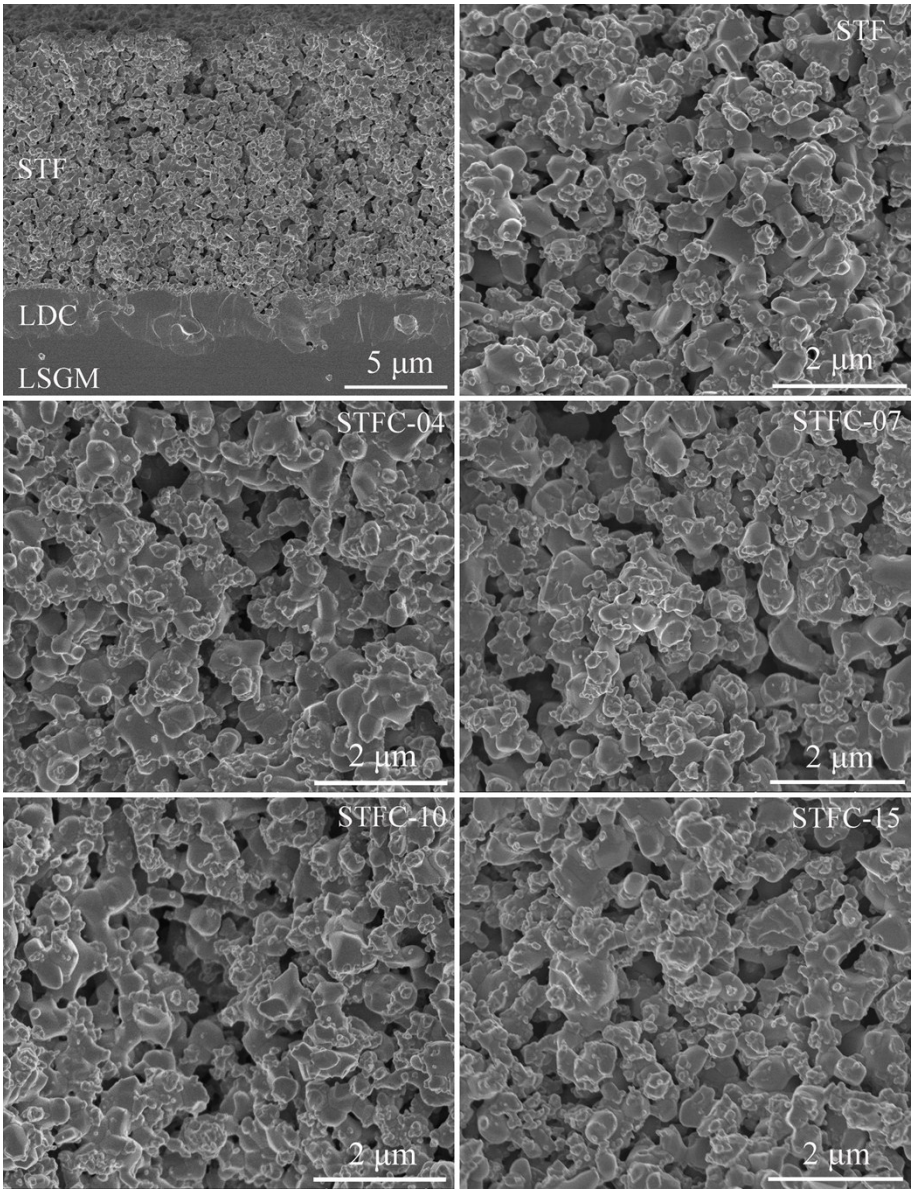

Fig. S2 Fractured surface morphologies for STF and STFC samples; (a) Low magnification image for STF; High magnification image for STF (b), STFC-04 (c), STFC-07 (d), STFC-10 (e), and STFC-15 (f).

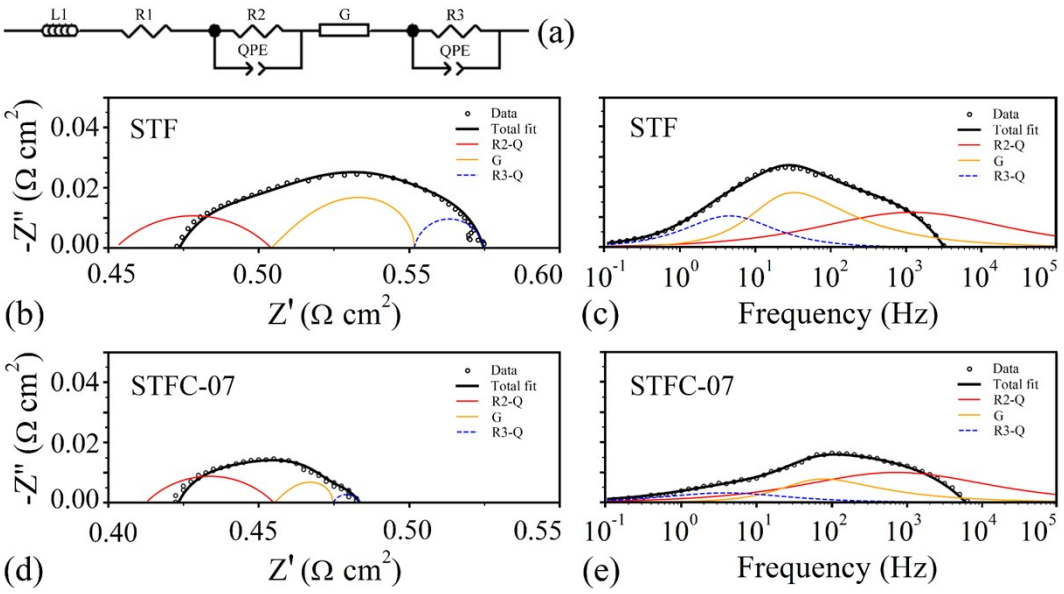

Fig. S3 Typical L-R-G EIS fittings for the symmetric cells at 700 °C. (a) equivalent circuit, (b) and (d) are the Nyquist plots of STF and STFC-07, respectively; (c) and (e) are the Bode plots for STF and STFC-07, respectively. Solid lines are the fitting results. Note that the inductance of test setup wires is not shown as a separate response in these plots, and is responsible for the apparent difference between the overall fit and the individual responses.

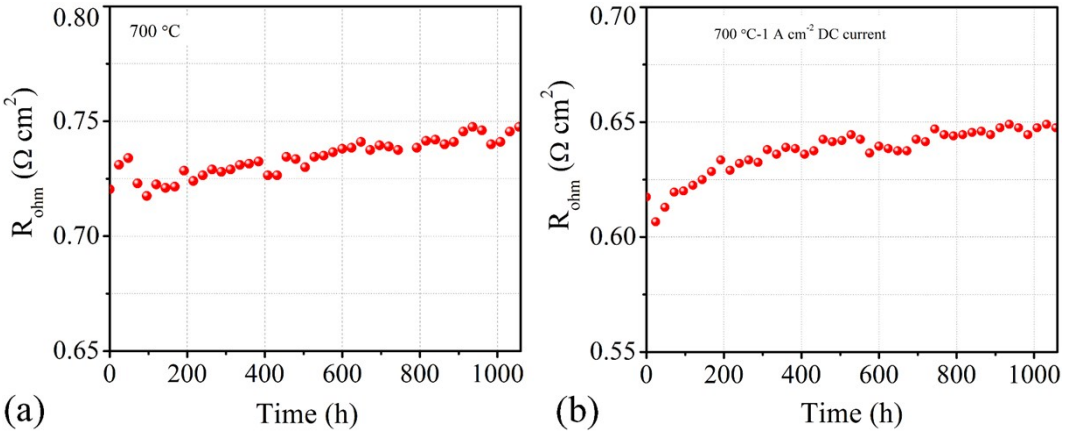

Fig. S4 Ohmic resistance versus time for the symmetric cells with STFC-07 electrodes during life testing; (a) without current; (b) running 1 A cm^{-2} current. A small difference between the initial values attributed to the small difference of the thickness of LSGM electrolytes.

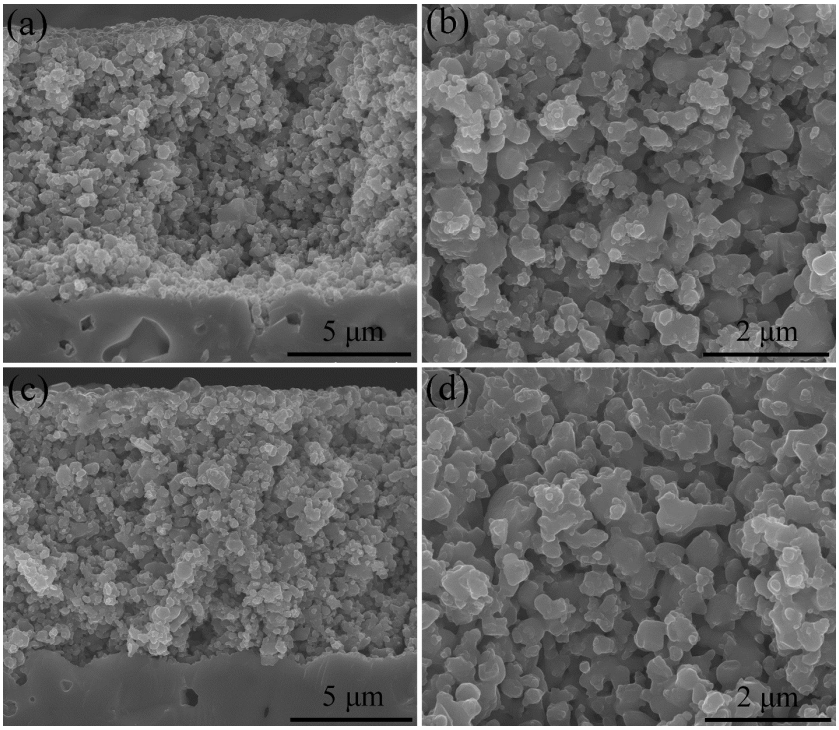

Fig. S5 Fractured surface morphologies for symmetric cells after the ageing (700 °C, without current). (a) and (b) for STF; (c) and (d) for STFC-07. (a) and (c) show the electrode/electrolyte interfaces.

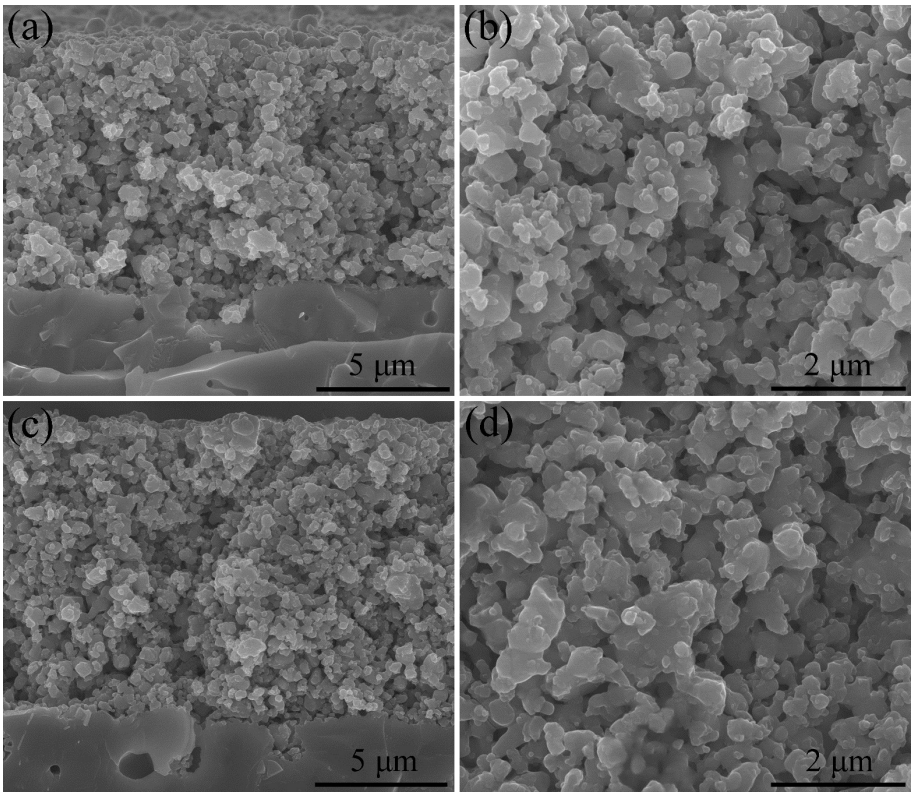

Fig. S6 Fractured surface morphologies of SOFC side for the symmetric cells after the ageing (700 °C, 1 A cm^{-2}). (a) and (b) for STF; (c) and (d) for STFC-07. (a) and (c) show the electrode/electrolyte interfaces.

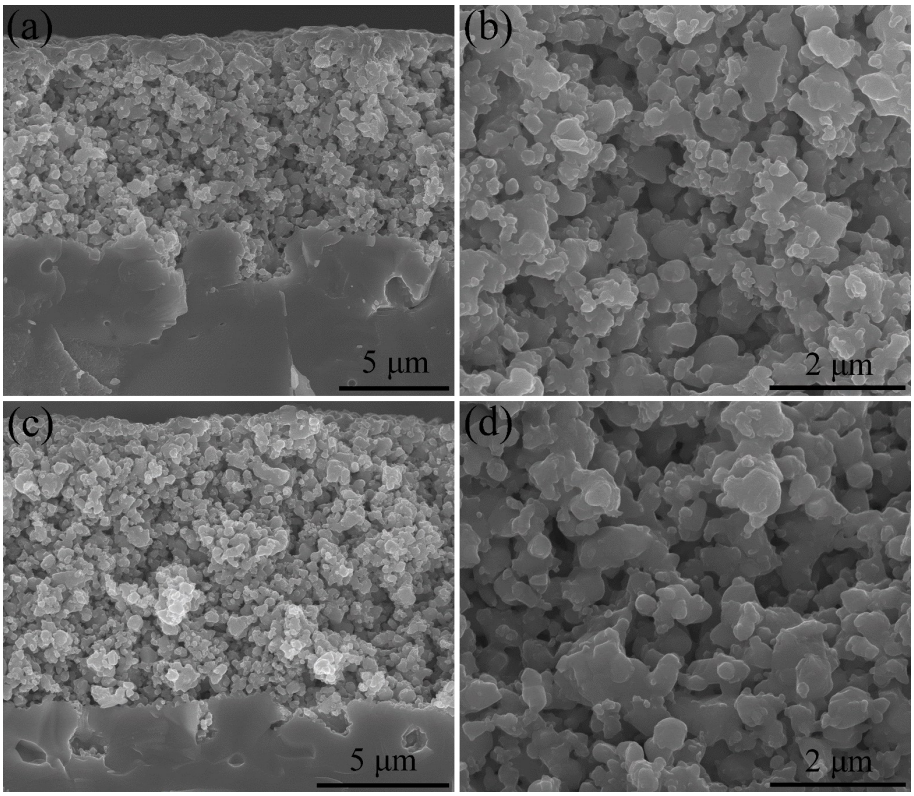

Fig. S7 Fractured surface morphologies of SOEC side for the symmetric cells after the ageing (700 °C, 1 A cm^{-2}). (a) and (b) for STF; (c) and (d) for STFC-07. (a) and (c) show the electrode/electrolyte interfaces.

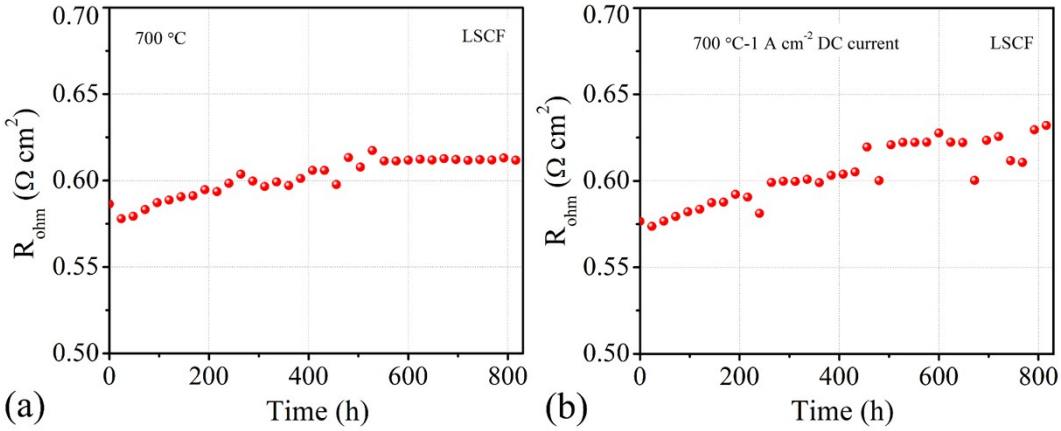

Fig. S8 Ohmic resistance versus time for the symmetric cells with LSCF electrodes; (a) without current; (b) running 1 A cm^{-2} DC current.

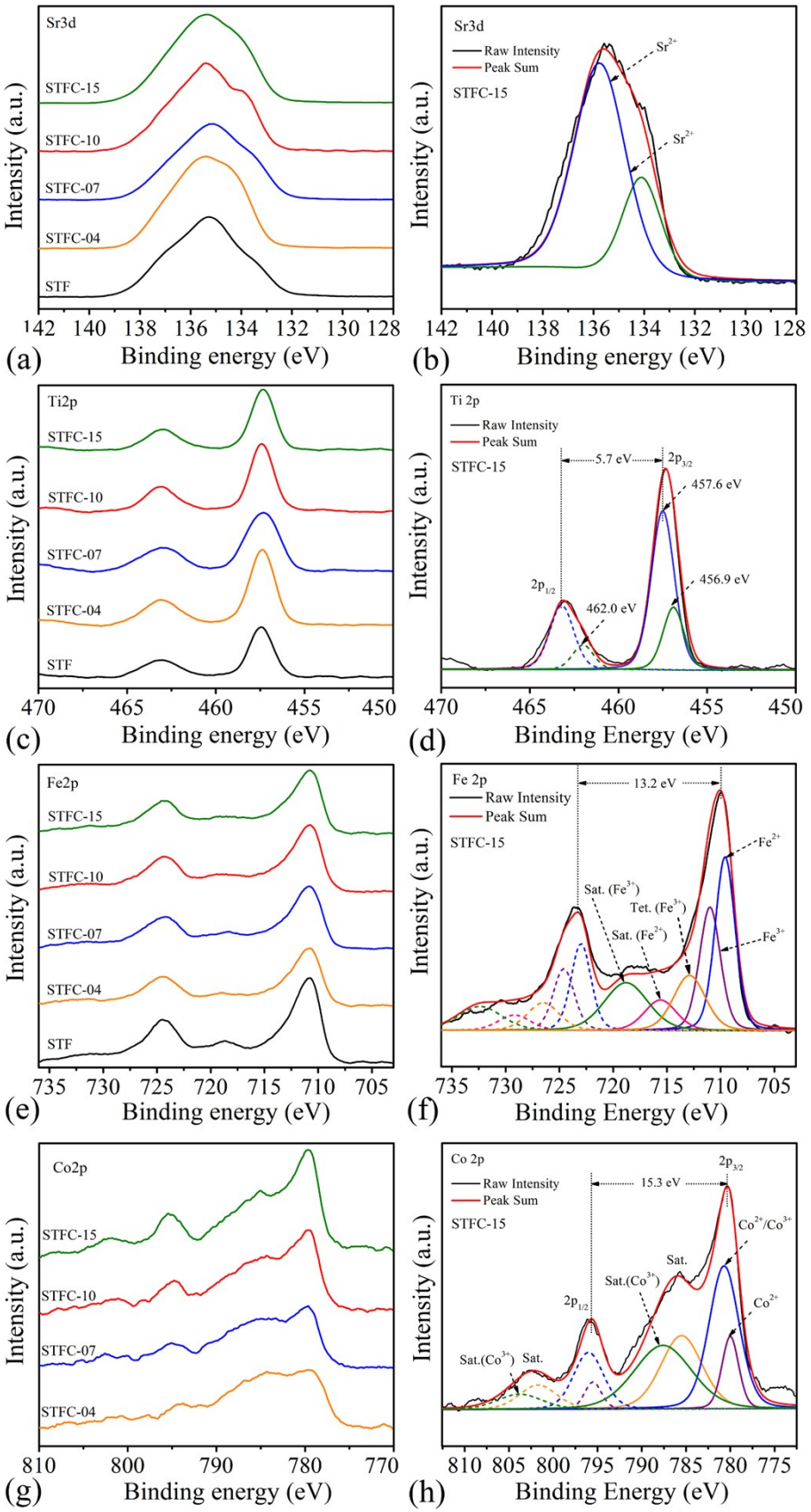

Fig. S9 XPS spectras for STF and STFC electrodes; narrow-scan for (a) Sr 3d, (c) Ti 2p, (e) Fe 2p, and (g) Co 2p; Fittings for STFC-15 samples: (b) Sr 3d, (d) Ti 2p, (f) Fe 2p, and (h) Co 2p

According to the high-resolution scans and their fittings, it observed that there are no big differences in peak positions for Sr and Ti between different samples and the measured binding energy for different elements are consistent with the values reported in the literature[1]. As expected, the peak intensity on Fe decreased and that of Co increased with increasing Co substitution.

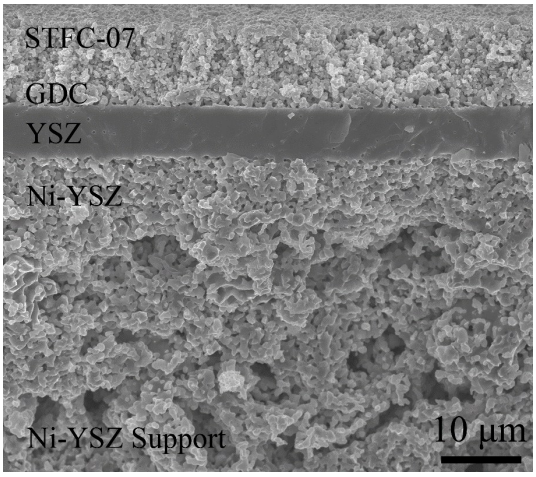

Fig. S10 Cross section SEM image of the full cell after performance testing

Fig. S10 shows a representative cross sectional SEM image of the full cell after the performance testing. The YSZ electrolyte has a thickness of about 8 μm and shows a very dense microstructure. The screen-printed STFC-07 electrode has a thickness of 10–15 μm and bonded well with the GDC interlayer. The Ni/YSZ fuel electrode and support layer have thicknesses of 15 and 700 μm, respectively.

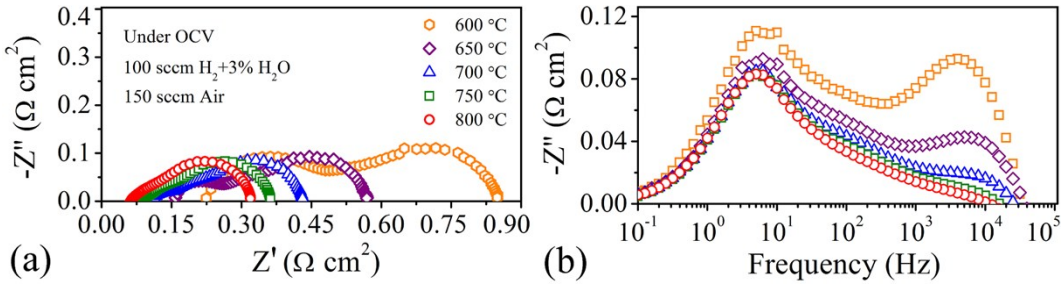

Fig. S11 Nyquist (a) and Bode plots for the full cell (3% H_2O + 97% H_2) at different temperatures.

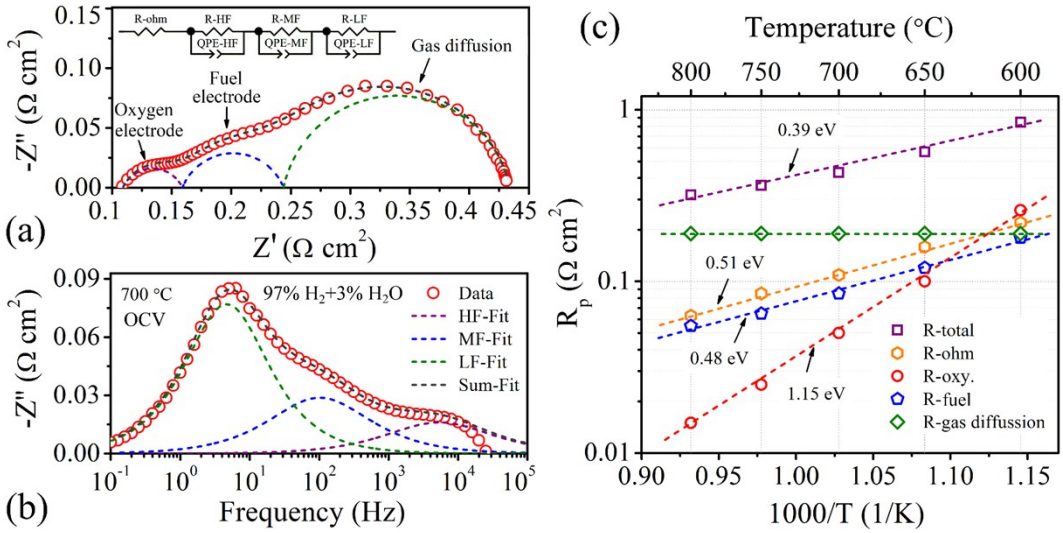

Fig. S12 Equivalent circuit fits for EIS data (700 °C, 3% H_2O + 50% H_2) from full cell; (a) Nyquist and (b) Bode plots, (c) Arrhenius plots of the polarization resistances from the fitting results for the full cell.

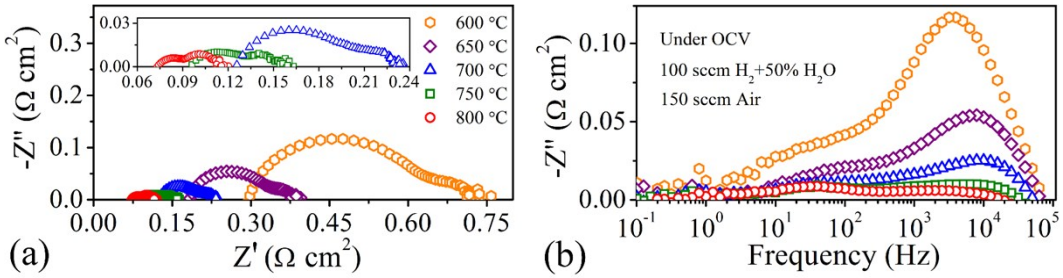

Fig. S13 Nyquist (a) and Bode plots for the full cell (50% H_2O + 50% H_2) at different temperatures.

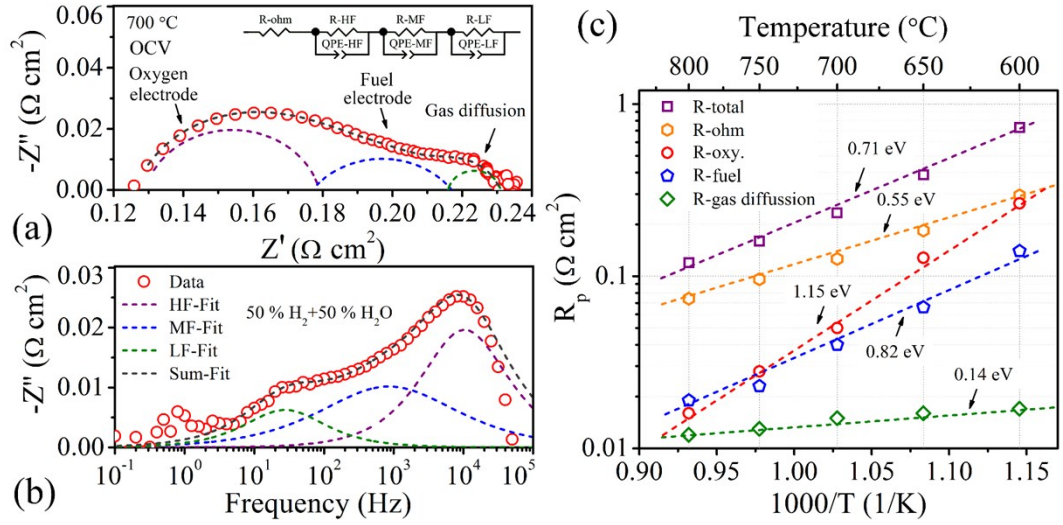

Fig. S14 Equivalent circuit fits for EIS data (700 °C, 50% H_2O + 50% H_2) from full cell; (a) Nyquist and (b) Bode plots, (c) Arrhenius plots of the polarization resistances from the fitting results for the full cell.

Discussion of the full cell EIS data

In the present study, the cell exhibited three clear impedance responses at all the temperatures. The EIS data was fit to an equivalent circuit consisting of three RQ elements, matching to the three different responses seen by visual inspection, an Ohmic resistance (R_{ohm}), and an inductor. Fig. S12 (a) and (b) shows typical fits, for data taken at 700 °C. The resistance values obtained from each circuit element are shown in the Arrhenius plots in Fig. S12 (c). The Ohmic resistance values are consistent with the magnitude expected for the YSZ electrolyte, although the activation energy is lower than expected. The response at ~10 Hz did not vary significantly with temperature (Fig. S11 (b)), and is therefore associated with gas diffusion in the thick support, consistent with prior reports.[2] The response peaking at ~10^2 is a combination of the oxygen electrode response, as seen in the EIS data for the cathode symmetric cell in Figure, and the Ni-YSZ fuel electrode electrochemical process normally observed at this frequency.[3] The response peaking at ~10^4 Hz is similar to the high frequency response seen in the cathode symmetric cell EIS data, but is larger in magnitude. This may be due to a difference in the processing between the symmetric in full cells, or there may be an additional interfacial resistance in the full cells that is not present in the symmetric cells.

EIS data, from the same cell as shown in Fig. 7, was measured in 3% H_2O + 97% H_2 fuel and air at open circuit voltage (OCV) at 600–800 °C. Nyquist and Bode plots, reproduced in Fig. S11, show three main responses at 10, 100, and 10^4 Hz that were fit with the equivalent circuit shown. The dominant feature, at ~10 Hz, does not vary significantly with temperature, as shown in the fitted resistance values (Fig. S12). This is commonly observed in Ni-YSZ anode-supported cells and can be attributed to gas diffusion through the thick (~700 μm) anode support. Gas diffusion is also presumably responsible for the limiting current observed at ~6 A cm^{-2} in Fig. 7. The resistance values from each part were obtained. The oxygen electrode polarization ($R_{-oxy.}$) showed the lowest value at temperatures of 800–650 °C and close to R_{ohm}, fuel electrode polarization (R_{-fuel}), and gas diffusion resistance ($R_{-gas\ diffusion}$) at 600 °C. The $R_{-oxy.}$ activation energy determined for the full cell in Fig. 7 (a) (1.15 eV) is similar to the value determined previously from the symmetric cell study in Fig. 4 (1.21 eV).

Nyquist and Bode plots from the same cell measured in 50% H_2O + 50% H_2 fuel and air at OCV at 600–800 °C are shown in Fig. S13. Similar fitting was produced and the results

are shown in Fig. S14. It also shows three main responses at the same frequency regions as shown in Fig. S12. Firstly, the total resistance values were 0.112, 0.233, and 0.598 Ω cm^2 at 800, 700, and 600 °C, respectively. On the other hand, it observed that the R_{-oxy} almost not change when the fuel steam concentration increased from 3% to 50% because the air gas on the oxygen electrode side not changed. However, the R_{-fuel} and $R_{-gas\ diffusion}$ decreased obviously since the high fuel steam concentration yields a lower fuel electrode polarization as discussed above.

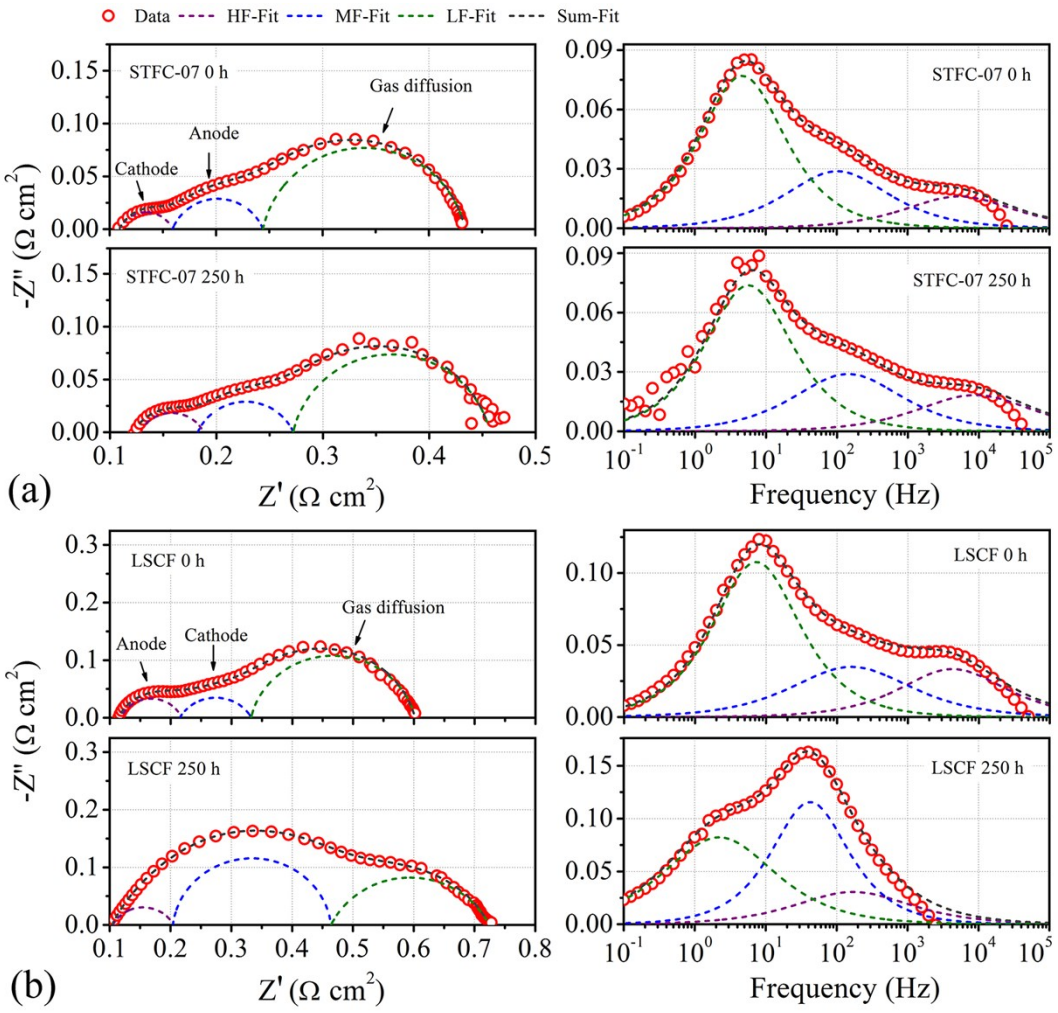

Fig. S15 Comparisons of EIS for full cells with STFC-07 and LSCF cathodes before and after SOFC life test. Test conditions: 700 °C, 1 A cm^{-2}/ 130 h + 1.2 A cm^{-2}/120 h.

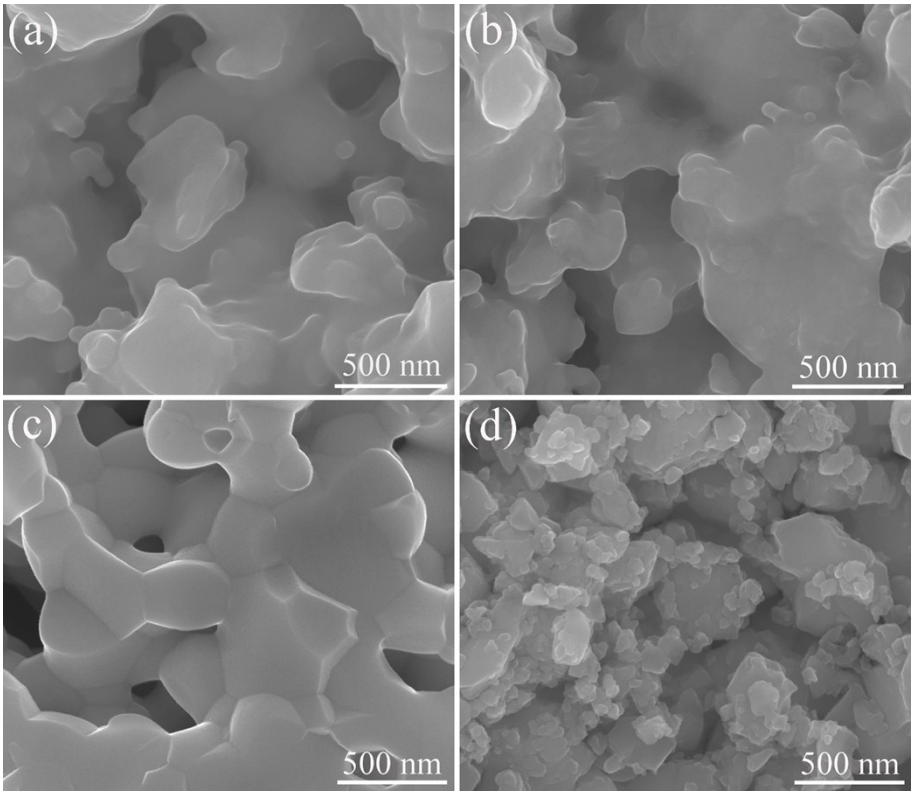

Fig. S16 (a) and (c) fractured surface morphologies for as-prepared STFC-07 and LSCF cathodes, respectively; (b) SFTC-07 after 350 h life testing (SOFC, 700 °C, 1 A cm^{-2}/ 130 h + 1.2 A cm^{-2}/120 h + 1.5 A cm^{-2}/100 h); (d) LSCF after 250 h life testing (SOFC, 700 °C, 1 A cm^{-2}/ 130 h + 1.2 A cm^{-2}/120 h)

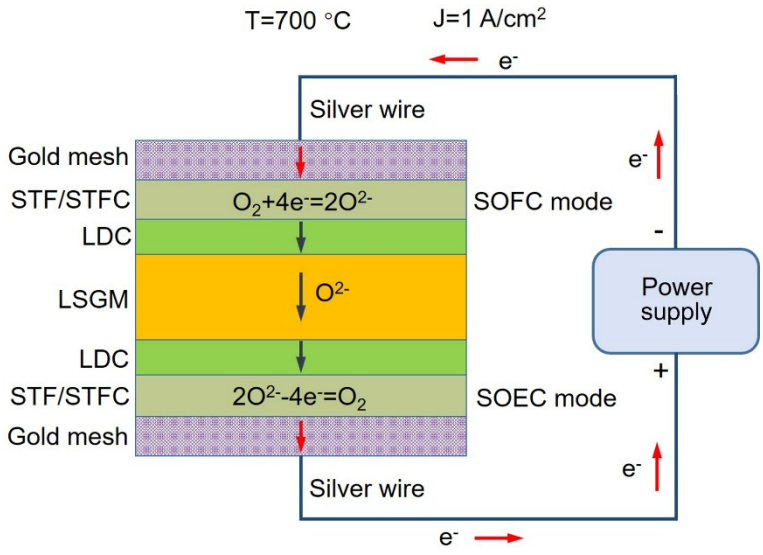

Fig. S17 The configuration of symmetrical cells and long-term stability test under a current supply.

Table S1 Gerischer resistance R_G (Ω cm^2) and time constant t_G (s) values obtained from fitting the EIS data and used in the ALS model calculations.

Temperature (°C)	R_G (STF)	R_G (STFC-07)	t_G (STF)	t_G (STFC-07)
600	0.282	0.113	0.0913	0.0422
650	0.131	0.045	0.0271	0.0091
700	0.054	0.021	0.0071	0.0028
750	0.026	0.0085	0.0022	0.0071
800	0.015	0.0045	0.0091	0.0029

Table S2 Oxygen nonstoichiometry (δ) and thermodynamic factors (A_0) from TGA analysis used for ALS mode.

Temperature (°C)	A_0 (STF)	A_0 (STFC-07)	δ (STF)	δ (STFC-07)
600	9.60	11.54	0.219	0.277
650	10.38	12.3	0.228	0.298
700	10.25	13.16	0.249	0.316
750	10.8	13.88	0.259	0.325
800	11.81	14.69	0.266	0.332

Adler-Lane-Steele (ALS) model

The ALS model[4, 5] was developed to describe the impedance response of porous single-phase MIEC oxides. It is applied in this work to help interpret EIS data and use it, combined with 3D tomography data, to extract the oxygen transport coefficients of STFC. The ALS model leads to a specific electrical equivalent circuit (Gerischer impedance element) with the form:

$$Z = R_G \sqrt{\frac{1}{1 + (j\omega t_G)^{\alpha}}} \tag{S1}$$

where Z is the complex impedance, R_G is the Gerisher resistance and t_G is the time constant. R_G and t_G are given by the ALS model as:

$$R_G = \frac{RT}{8F^2} \sqrt{\frac{\tau A_0^2}{\alpha(1-\varepsilon) D_{chem} k_{chem} \delta c_{mc}^{\,2}}} (pO_2)^{-0.25} \tag{S2}$$

$$t_G = \frac{\delta(1-\varepsilon)}{4\alpha k_{chem}}(pO_2)^{-0.5} \quad \text{(S3)}$$

where τ is the tortuosity, ε is the porosity of solid phase, and α is the pore-electrode interfacial area per volume. These values are given in Fig. 2(d) from the FIB-SEM data. c_{mc} is the oxygen concentration. δ is the oxygen vacancy fraction. A_0 is the thermamodynamic factor, a function of oxygen chemical potential.

$$A_0 = \pm\frac{1}{2}\left(\frac{\partial ln(PO_2)}{\partial ln(\delta)}\right) \quad \text{(S4)}$$

RG and tG are determined from the EIS fitting shown in Fig. S2 and the values are shown in Table Si. A_0 was calculated from Fig. 1(c). δ and A_0 used in present study are shown in Table S2.

According to eq. (a) and (3), D_{chem} and k_{chem} can be obtained:

$$D_{chem} = \left(\frac{RT}{4F^2R_G}\right)^2 \frac{\tau A_0^2 t_G}{(1-\varepsilon)^2 c_{mc}^2 \delta^2} \quad \text{(S5)}$$

$$k_{chem} = \frac{(1-\varepsilon)\delta}{4\alpha t_G}(pO_2)^{-0.5} \quad \text{(S6)}$$

Reference

1. O. Lobacheva, Y. M. Yiu, N. Chen, T. K. Sham and L. V. Goncharova, *Appl. Surf.Sci.,* 2017, **393**, 74.
2. Z. Gao, V. Y. Zenou, D. Kennouche, L. Marks and S. A. Barnett, *J. Mater. Chem. A*, 2015, **3**, 9955.
3. D. Kennouche, Y.-c. K. Chen-Wiegart, J. S. Cronin, J. Wang and S. A. Barnett, *J. Electrochem. Soc.*, 2013, **160**, F1293.
4. J. Railsback, G. Hughes, L. Mogni, A. Montenegro-Hernández and S. Barnett, *J. Electrochem. Soc.*, 2016, **163**, F1433.
5. K. Yakal-Kremski, L. V. Mogni, A. Montenegro-Hernández, A. Caneiro and S. A. Barnett, *J J. Electrochem. Soc.*, 2014, **161**, F1366.